



# CHORUS

This is the accepted manuscript made available via CHORUS. The article has been published as:

## Superfluidlike Mass Flow Through 8 $\mu\text{m}$ Thick Solid $^4\text{He}$ Samples

Jaeho Shin, Duk Y. Kim, Ariel Haziot, and Moses H. W. Chan

Phys. Rev. Lett. **118**, 235301 — Published 9 June 2017

DOI: [10.1103/PhysRevLett.118.235301](https://doi.org/10.1103/PhysRevLett.118.235301)

# Superfluid-like mass flow through 8 $\mu\text{m}$ thick solid $^4\text{He}$ samples

Jaeho Shin, Duk Y. Kim,\* Ariel Haziot,<sup>†</sup> and Moses H. W. Chan<sup>‡</sup>

*Department of Physics, The Pennsylvania State University,  
University Park, Pennsylvania 16802-6300, USA*

(Dated: May 15, 2017)

We report the observation of superfluid-like mass flow through coin-shaped 8  $\mu\text{m}$  thick solid  $^4\text{He}$  samples sandwiched between superfluid leads. Mass flow is found from the melting pressure to at least 30 bar with a concomitant decrease in the onset temperature from 1 K to 0.25 K. The mass flow rate is found to be sample dependent and can be enhanced by thermal annealing. The flow rate decreases with temperature and decays nearly exponentially with the pressure of the samples. The dissipation associated with the mass flow decreases with temperature and becomes superfluid-like near 0.1 K. In contrast to earlier studies on centimeter-thick samples, we do not see a sharp cut-off in the mass flow rate at low temperature.

Recent experiments at the University of Massachusetts (UM) found evidence of superfluid-like mass flow through 4 cm thick solid  $^4\text{He}$  samples sandwiched between superfluid leads in the form of porous Vycor cylinders filled with superfluid  $^4\text{He}$  [1–4]. Due to the small pores in Vycor, the freezing pressure of  $^4\text{He}$  inside Vycor is elevated to 35 bar [5] and enables a superfluid/solid/superfluid sample geometry. The UM experiments found mass flow below 625 mK and 27 bar in some but not all solid samples. Many of the features found at UM were replicated at the University of Alberta (UA) by directly compressing the solid [6, 7]. These observations have been interpreted as consequences of the ‘superclimb’ process where edge dislocations with superfluid core transport  $^4\text{He}$  from superfluid into the solid and through the solid [8–10] and/or transport through the superfluid cores of screw dislocations [11].

We studied mass flow through 8  $\mu\text{m}$  thick solid  $^4\text{He}$  samples with the same sandwich geometry (inset of Fig. 1 and Supplementary Material I [12]). Since 8  $\mu\text{m}$  is shorter than the typical length of dislocations [17, 18], the dislocation lines are likely pinned at the two flat surfaces of the solid sample and aligned primarily along the flow path direction [19] without forming a network as in prior centimeter-thick solid samples. Fig. 1 summarizes the results of this study: namely superfluid-like mass flow is found to the left of dashed curve.

The 8  $\mu\text{m}$  sample space inside a copper casing is subtended by a Kapton foil with a circular open aperture pressed between two Vycor cylinders. The copper casing thermally anchored to the mixing chamber keeps the low temperature ends of Vycor cylinders and the solid sample at the same temperature. The high temperature ends of the Vycor cylinders open to small volumes *SL* and *SR* and are then connected by capillaries to the piezoelectric pressure gauges *PL* and *PR* and to the  $^4\text{He}$  gas handling system at room temperature. *SL* and *SR* serve as reservoirs for bulk liquid  $^4\text{He}$ .

Three different procedures are used to grow solid samples. In the first method, a flow field is created by continuously feeding  $^4\text{He}$  gas into the cell from one capillary

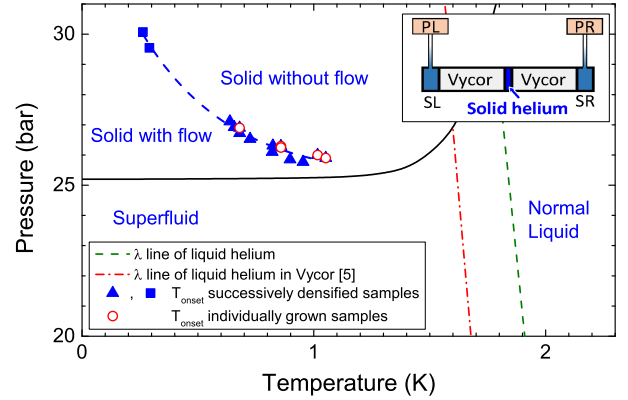


FIG. 1. Boundary of mass flow phenomenon in solid  $^4\text{He}$ . Mass flow is found to the left of the dashed blue curve defined by  $T_{\text{onset}}$ , the onset temperatures extrapolated from mass flow vs. temperature data from Fig. 4. The blue dashed curve is a simple exponential fitting of the  $T_{\text{onset}}$  data. Inset: Schematic drawing of the sample cell.

and vented via the other that allows the growth of a solid sample from superfluid in the 8  $\mu\text{m}$  gap to the intended pressure. In the second method, a solid sample is grown from superfluid in the absence of a flow field by feeding helium into the cell symmetrically from both capillaries. In the third method, liquid samples were refrozen near 1.5 K without adding helium. All 80 samples grown and densified by the first method between 70 mK and 1 K showed mass flow. In comparison, 10 out of 13 solid samples grown by the second method showed mass flow and only 3 out of 10 samples refrozen from liquid showed mass flow. The flow rates both prior to and after thermal annealing are sample dependent. More details are shown in Supplementary Material II.

Two different procedures are used to induce flow through the samples. In the piston method,  $^4\text{He}$  gas is injected via one of the capillaries into the cell and the flow rate is determined by monitoring *PL* and *PR*. The injection is accomplished by reducing momentarily the room temperature volume next to *PL* (or *PR*). Fig. 2(a)

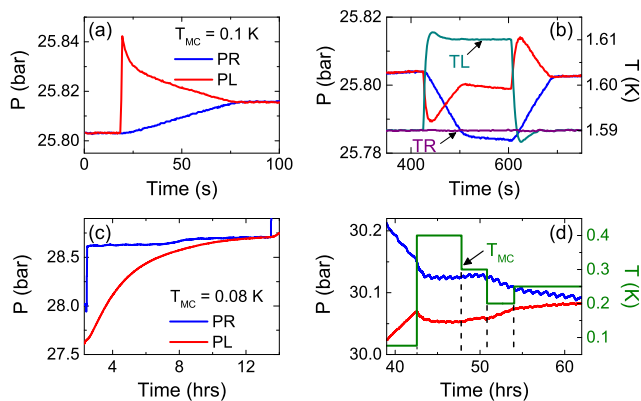


FIG. 2. Time evolution of  $PR$  and  $PL$  in response to (a) the injection of  $^4\text{He}$  gas to the left of sample cell at  $t = 19$  s; (b) the introduction (at  $t = 425$  s) and removal (at  $t = 605$  s) of a 20 mK heat pulse on  $SL$ . Flow rates shown in panels (a) and (b) are identical at 0.23 mbar/s. (c) The exponential approach of  $PL$  towards a constant  $PR$  indicates the mass flow is limited by the normal fluid inside Vycor. (d)  $PL$  and  $PR$  equilibrate towards each other after an injection of  $^4\text{He}$  gas to the right side of a 30.1 bar sample. The mass flow rate decreases with temperature between 0.1 to 0.25 K. No evidence of flow above 0.3 K. Pressure oscillations came from oscillations of the still temperature.

shows the time evolution of  $PR$  and  $PL$  in response to a sudden increase in  $PL$  for a solid sample at 25.8 bar. An immediate linear increase is seen in  $PR$ . For  $PL$ , there is an initial rapid drop followed by a gradual linear decrease that matches the increase in  $PR$ . The initial rapid drop is the result of the room temperature  $^4\text{He}$  gas condensing into  $SL$ . The subsequent linear decrease in  $PL$  and the matching linear increase in  $PR$  indicate a constant left to right mass flow that is independent of  $(PL - PR)$ . The flow ends abruptly when  $PL = PR$ .

Fig. 2(b) shows mass flow through the same solid sample induced by fountain pressure. The linear decrease in  $PR$  observed at the introduction of  $\delta T = 20$  mK to  $SL$  is due to mass flow from right to left through the sample. The initial drop in  $PL$  at  $t = 425$  s in response to the introduction of  $\delta T$  is due to a ‘secondary’ fountain effect between  $SL$  and the superfluid in the capillary on the left. The heat imposed on  $SL$  creates a fountain pressure that pulls liquid  $^4\text{He}$  from the capillary and reduces the pressure in the room temperature volume near  $PL$ . After a new temperature profile along the capillary is established near  $t = 440$  s,  $PL$  proceeds to increase linearly at a rate that matches precisely the decrease shown by  $PR$ . The responses in  $PL$  and  $PR$  after the removal of  $\delta T$  are mirror opposites of that seen due to the introduction of  $\delta T$ .

In our sandwich configuration, the measured mass flow rate is limited by and yields the flow rate of the ‘bottleneck’ along the flow path. Solid samples with pressure below 27.3 bar are usually the bottlenecks since  $SL$  and

$SR$ , as well as the Vycor cylinders are filled with superfluid. Interestingly, at sample temperature near 0.1 K and under a very small  $\delta T$ , superfluid in Vycor cylinders is the bottleneck instead of the solid sample (Supplementary Material III). For measurements of solid samples above 27.3 bar, it is necessary to control both  $SR$  and  $SL$  at temperatures higher than 1.65 K to keep  $^4\text{He}$  in the reservoirs from solidifying. This drives the  $^4\text{He}$  in the high temperature ends of the Vycor cylinders into the normal phase (see Fig. 1). As a result, the Vycor cylinders become the bottlenecks of the flow path for pressure between 27.3 bar and 29 bar and the mass flow through the solid cannot be measured. Since the flow rate decays nearly exponentially and rapidly with pressure (Fig. 5), solid samples with pressure above 29.5 bar replace the Vycor as the bottlenecks and their flow rate can be measured again.

Fig. 2(c) and 2(d) show mass flow of solid samples at 28.5 and 30.1 bar and illustrate the ‘bottleneck’ phenomenon. For the 28.5 bar sample,  $PR$  is raised and kept at a nearly constant value.  $PL$  is found to increase exponentially towards  $PR$  with a time constant of 4 hours. Such an exponential equilibration is what one would expect if the impedance of mass flow is dominated by normal fluid in the high temperature ends of the Vycor cylinders. Piston method is used to induce flow on the 30.1 bar sample labeled as sample TH03 in Fig. 4. The mass flow rate (independent of time) is found to decrease with increasing temperature up to 0.25 K. No flow is found at 0.3 or 0.4 K.

Reference 2 reported sub-linear dependence of flow rate on the chemical potential difference across the two bulk liquid reservoirs and the result was interpreted as evidence of Luttinger-liquid like transport. We found similar behavior. At low  $\delta T$  mass flow rate increases linearly with  $\delta T$  and above a certain value of  $\delta T$ , a sub-linear

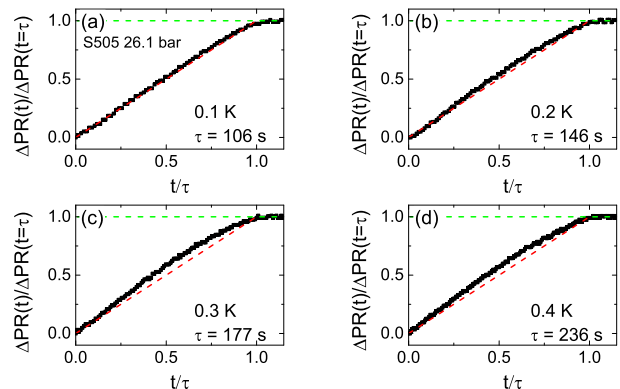


FIG. 3. Responses of the change in  $PR$  ( $\Delta PR$ ) vs. time ( $t$ ) of sample S505 at 0.1, 0.2, 0.3 and 0.4 K immediately after the removal of heat pulse. Equilibrium is reached at  $t = \tau$  when  $PR = PL$ . The red dashed straight lines highlight the onset of curvature in  $PR$  vs. time that appears above 0.1 K.

dependence is found (Supplementary Material III). We examine closely the time evolution of  $PR$  in response to the removal of the heat ( $\delta T$ ) imposed on  $SL$ . Fig. 3 shows the fractional change of  $PR$  as a function of  $t/\tau$  at 4 different temperatures, with  $\tau$  being the time when  $PR$  becomes equal to  $PL$  at the end of mass flow. At 0.1 K,  $PR$  is found to increase towards  $PL$  linearly with time with no noticeable deviation. This means the flow rate is a constant independent of the pressure difference and ends abruptly when  $PR = PL$ . This is consistent with dissipationless superflow. At higher temperature the flow rate decreases with time. Consistent results on other samples are shown in Supplementary Material IV. It would be interesting to ascertain by a more definitive method if the mass flow is truly dissipationless near and below 0.1 K.

Contrary to UM [3, 4], we found thermal annealing enhances instead of diminishes the flow rate. When a sample grown near 0.1 K is annealed up to 0.8 K, a saturated and reproducible (upon warming and cooling) flow rate is found. The enhancement ranges from 30% to 400%. Solid samples grown near and above 0.8 K, as expected, require no annealing to be in the saturated state. More details are shown in Supplementary Material V. The reported flow rates in this paper are the ‘saturated’ values from samples grown in the presence of a flow field and measured by fountain effect with a  $\delta T = 20$  mK.

Fig. 4 shows flow rate decreases with temperature in 16 solid samples. This trend is consistent with the UM results. A flow rate of 100 ng/s corresponds to a time rate of change in  $PR$  or  $PL \approx 0.34$  mbar/s (Supplementary Material I). Sample TS5 was grown with  $^4\text{He}$  gas with 5 parts per trillion (ppt) of  $^3\text{He}$  from superfluid at 70 mK and annealed to 0.8 K. Samples TS6 through TS13 were sequentially densified at 70 mK and measured. The piston method was used for samples TH01 and TH03 at 29.6 and 30.1 bar. The flow rates of the densified solid samples decrease with pressure and show reproducible temperature dependence upon warming and cooling without any additional thermal annealing. It appears these densified solid samples ‘inherit’ the changes imparted into TS5 when it was annealed. The inset shows that the decrease with temperature in the flow rate accelerates with the sample pressure. The result of the 26.4 bar sample from UM [4] is also shown in the inset for comparison.

In addition to the TS and TH samples, Fig. 4 also shows flow rate vs. temperature for samples S08, S10, S11, He3c and He3f. S08, S10 and S11 were individually grown from superfluid and annealed to 0.8 K. The magnitude of the flow rate of S08 is significantly lower than S10, TS5 and TS6, samples at comparable pressure. This illustrates that the flow rate is sample dependent even after thermal annealing (Supplementary Material II). Samples He3c and He3f were grown with gas mixtures with  $X_3$  equal to 16 and 1200 ppm. The results of seven other solid samples made with gas mixtures with

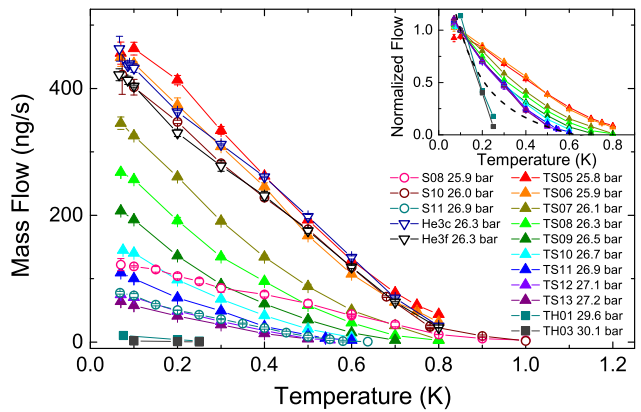


FIG. 4. Mass flow rate vs. temperature of solid samples at different pressures. Normalized mass flow rates (flow rate at 0.1 K = 1) of the TS and TH samples are shown in the inset. Result from a UM sample at 26.4 bar [4] is shown in the inset as a dashed curve.

$X_3$  that ranges from 5 ppt to 1.5% are shown in Supplementary Material VI. This series of measurements were made to search for the sharp-drop in flow rate at low temperature found at UM and UA [3, 4, 6, 7]. We found no sign of such a drop down to 70 mK in any of these samples. This discrepancy is consistent with the idea [4] that the sharp-drop is the consequence of the binding of  $^3\text{He}$  at the junctions of the dislocation lines. These junctions are absent in our thin samples. The addition of  $^3\text{He}$  impurities also does not alter the temperature dependence or the magnitude of the flow rate.

Fig. 5 shows mass flow rate at 0.1 K as a function of the pressure of the solid samples. Each of the five data sets labeled as SA to SE began with a fresh low pressure ‘seed’ solid sample grown from superfluid under a flow field at 0.1 K. After the flow rate of the seed sample was measured at 0.1 K, it was densified to higher pressure and measured without thermal annealing. The data set shown in black triangles is extracted from Fig. 4. Flow rate vs. pressure of two series of samples using  $^4\text{He}$  gas with 1200 ppm of  $^3\text{He}$  are also shown. The seed solid sample of one of these series was thermally annealed and the other was not. Fig. 5 shows that an exponential function provides a good description of the dependence of mass flow rates on pressure. However, different flow rates and decay constants are found for each of the nine data sets. The open symbols in data sets SC and SD came from samples depressurized from a prior sample of higher density. These data demonstrate an absence of ‘pressure’ or ‘densification’ hysteresis in flow rate and decay constant. It appears the mass flow rate and the decay constant are determined by some specific properties that were ‘imprinted’ into the seed solid sample when it was initially grown from superfluid. The orientation and size of the crystal grains and the ‘kinks’ and ‘jogs’ [22] of the dislocation lines are possible ‘imprintable’ properties

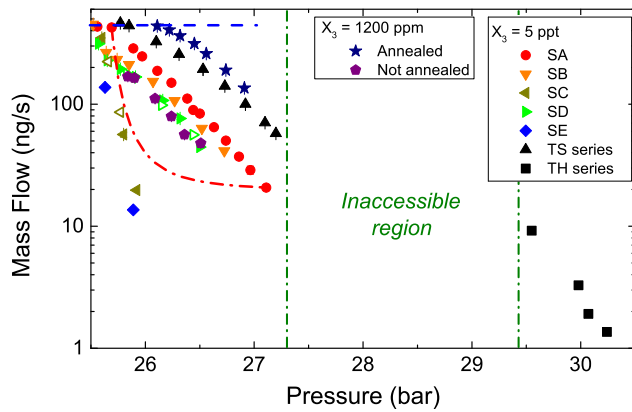


FIG. 5. Mass flow rate measured at 0.1 K as a function of sample pressure. The flow rate of superfluid through the Vycor cylinders at 450 ng/s is marked by a blue horizontal dashed line (See supplementary Materials III). This sets the upper limit of the observed flow rate. When the data at and near this saturated value are excluded, the flow rates of all nine sequences of samples, show nearly exponential decay with pressure. Decay constants and flow rate show sample-to-sample variation. The Vycor ‘bottleneck’ effect prevents the measurement of flow rate of samples between 27.3 and 29.5 bar. The red dashed-dotted curve represents a quadratic dependence of flow rate on pressure  $P$  (rate =  $A_0(P-P_m)^{-2} + B_0$ ).  $P_m$  is the melting pressure and  $A_0$  and  $B_0$  are constants determined by anchoring the curve at two data points of the SA sequence. Such a quadratic dependence is predicted if liquid channels are responsible for the mass flow [20, 21].

that are passed on from the seed to the densified solid samples. Thermal annealing changes some but not all the imprinted properties (e.g. reducing the number of ‘jogs’ [22]) for higher flow rate.

A recent experiment studying superfluid  $^4\text{He}$  confined in porous Gelsil glass of 2.5 nm pore diameter found the superfluid transition temperature decreases with pressure beyond the bulk melting curve [23]. The superfluid boundary near 30 bar matches the dashed line shown in Fig. 1. The superfluid density vs. temperature plot also resembles the mass flow curves shown in Fig. 4. These resemblances raise the possibility that the observed mass flow in solid is a consequence of  $\sim 2.5$  nm diameter liquid channels [20, 21] percolating inside the solid. Our measured flow rate of 300 ng/s is equivalent to a solid/liquid  $^4\text{He}$  volume flow rate of above  $1.4 \times 10^{-6}$  cm<sup>3</sup>/s. This rate is the product of the cross section of the aperture ( $\pi(0.15)^2$  cm<sup>2</sup>), the superfluid density  $\rho_s$  and the flow velocity,  $v$ . If liquid channels are responsible for the mass flow, then  $\rho_s$  is equal to the density of the channels times the cross sectional area of each channel. The density of the channel then must exceed  $2 \times 10^7$  cm<sup>-2</sup> to give a reasonable (i.e.  $\sim 1$  m/s) superfluid velocity. Such a density implies the solid samples are consists of micron size crystallites instead of relatively large crystals expected for samples grown from superfluid [21]. It would

also predict a flow rate that decreases quadratically with pressure [20, 21]. Such a dependence, as shown in Fig. 5 is not seen. It has been suggested that grain boundaries are superfluid and may be responsible for the observed mass flow [24]. If this is the case, one would expect (as with the liquid channel scenario) thermal annealing should reduce rather than enhance the flow rate. In addition, one would also expect the mass flow rate to exhibit Kosterlitz-Thouless-like temperature dependence. This is also not seen.

The results of this experiment favor the superfluid screw dislocation model of mass flow. Since the edge dislocations are likely pinned nearly parallel to the flow path [19], the superclimb mechanism within the solid should not contribute to mass flow. If the superfluid core of screw dislocations are the conduits of the mass flow, then  $\rho_s$  is equal to an effective cross-sectional area of the superfluid core ( $\sim 1$  nm<sup>2</sup>) [8] times the density of dislocation. If we use  $10^5$  to  $10^6$  cm<sup>-2</sup>, the density found in shear modulus measurements [17, 18], a  $\rho_s$  that ranges from  $10^{-9}$  to  $10^{-8}$  is found. This would require a flow velocity  $v$  in the range of 150 to 1500 m/s to arrive at a flow rate of 300 ng/s. This may be reasonable since ‘inside’ a dislocation core the critical velocity can be on the order of the velocity of sound of solid  $^4\text{He}$  ( $\sim 500$  m/s). However, the weak path length dependence in the mass flow rate is somewhat puzzling within the superfluid screw dislocation model. The typical flow rate found in the UM experiment with a sample path length of 4 cm is 100 ng/s which is only 3 to 4 times smaller than what we found for a sample of 8  $\mu\text{m}$ .

The sample dependent and thermal annealing sensitive flow rates suggest the orientation of the  $^4\text{He}$  crystals and the dislocation lines within the crystals may be the key ‘imprinted’ properties of the samples. It will be worthwhile to study solid samples where the  $c$ -axes are aligned parallel and perpendicular to the flow field [25].

We thank John Beamish, Zhi-gang Cheng, R.B. Hallock, I. Iwasa, Jainendra Jain, A.B. Kuklov, and Nikolay Prokof'ev for informative discussions. We thank John Beamish for providing the isotopically pure  $^4\text{He}$  gas. This research is supported by NSF under grant DMR-1103159.

\* MPA-CMMS, Los Alamos National Laboratory, Los Alamos, New Mexico 87545, USA

† Institut NEEL, 38042 Grenoble cedex 9, France

‡ Corresponding author: MHC2@psu.edu

- [1] M. W. Ray and R. B. Hallock, Phys. Rev. Lett. **100**, 235301 (2008).
- [2] Y. Vekhov and R. B. Hallock, Phys. Rev. Lett. **109**, 045303 (2012).
- [3] Y. Vekhov, W. Mullin, and R. B. Hallock, Phys. Rev. Lett. **113**, 035302 (2014).

- [4] Y. Vekhov and R. Hallock, Phys. Rev. B **92**, 104509 (2015).
- [5] E. D. Adams, K. Uhlig, Y.-H. Tang, and G. E. Haas, Phys. Rev. Lett. **52**, 2249 (1984).
- [6] Z. G. Cheng, J. Beamish, A. D. Fefferman, F. Souris, S. Balibar, and V. Dauvois, Phys. Rev. Lett. **114**, 165301 (2015).
- [7] Z. G. Cheng and J. Beamish, Phys. Rev. Lett. **117**, 025301 (2016).
- [8] S. G. Soyler, A. B. Kuklov, L. Pollet, N. V. Prokof'ev, and B. V. Svistunov, Phys. Rev. Lett. **103**, 175301 (2009).
- [9] A. Kuklov, L. Pollet, N. Prokof'ev, and B. Svistunov, Phys. Rev. B **90**, 184508 (2014).
- [10] A. B. Kuklov, Phys. Rev. B **92**, 134504 (2015).
- [11] M. Boninsegni, A. B. Kuklov, L. Pollet, N. V. Prokofev, B. V. Svistunov, and M. Troyer, Phys. Rev. Lett. **99**, 035301 (2007).
- [12] See Supplemental Material at [url], which includes Refs. [13-16], for details about cell structure, sample dependence, sub-linear dependence, time evolution, thermal annealing effect, and  $^3\text{He}$  effect.
- [13] C. W. Kiewiet, H. E. Hall, and J. D. Reppy, Phys. Rev. Lett. **35**, 1286 (1975).
- [14] E. H. Graf, D. M. Lee, and J. D. Reppy, Phys. Rev. Lett. **19**, 417 (1967).
- [15] C. L. Kane and M. P. A. Fisher, Phys. Rev. Lett. **68**, 1220 (1992).
- [16] Y. Vekhov and R. B. Hallock, Phys. Rev. B **90**, 134511 (2014).
- [17] A. Haziot, A. D. Fefferman, J. R. Beamish, and S. Balibar, Phys. Rev. B **87**, 060509 (2013).
- [18] F. Souris, A. D. Fefferman, H. J. Maris, V. Dauvois, P. Jean-Baptiste, J. R. Beamish, and S. Balibar, Phys. Rev. B **90**, 180103 (2014).
- [19] Y. Aoki, I. Iwasa, T. Miura, A. Yamaguchi, and Y. Okuda, J. Low Temp. Phys. **183**, 113 (2016).
- [20] S. Sasaki, F. Caupin, and S. Balibar, Phys. Rev. Lett. **99**, 205302 (2007).
- [21] S. Sasaki, F. Caupin, and S. Balibar, J. Low Temp. Phys. **153**, 43 (2008).
- [22] F. Souris, A. D. Fefferman, A. Haziot, N. Garroum, J. R. Beamish, and S. Balibar, J. Low Temp. Phys. **178**, 149 (2015).
- [23] K. Yamamoto, H. Nakashima, Y. Shibayama, and K. Shirahama, Phys. Rev. Lett. **93**, 075302 (2004).
- [24] L. Pollet, M. Boninsegni, A. B. Kuklov, N. V. Prokof'ev, B. V. Svistunov, and M. Troyer, Phys. Rev. Lett. **98**, 135301 (2007).
- [25] S. Ramesh and J. D. Maynard, Phys. Rev. Lett. **49**, 47 (1982).